NATIONAL ADVISORY COMMITTEE FOR AERONAUTICS

WARTIME REPORT

ORIGINALLY ISSUED
August 1944 as
Advance Confidential Report L4E05

EFFECT ON HELICOPTER PERFORMANCE OF MODIFICATIONS IN PROFILE-DRAG CHARACTERISTICS OF ROTOR-BLADE AIRFOIL SECTIONS

By F. B. Gustafson

Langley Memorial Aeronautical Laboratory
Langley Field, Va.

NACA

WASHINGTON

NACA ACR No. L4H05

NATIONAL ADVISORY COMMITTEE FOR AERONAUTICS

ADVANCE CONFIDENTIAL REPORT

EFFECT ON HELICOPTER PERFORMANCE OF MODIFICATIONS IN PROFILE-DRAG CHARACTERISTICS OF ROTOR-BLADE AIRFOIL SECTIONS

By F. B. Gustafson

SUMMARY

Performance calculations are presented for a typical helicopter rotor in which three types of airfoil section were successively used. The types represented are the rough conventional, the smooth conventional, and the laminar-flow or low-drag sections as developed for helicopter use. The performance items covered are rotor thrust for fixed power in hovering, range and endurance at cruising speed, and power required at a relatively high forward speed. Contours showing the conditions of operation encountered by the blade section and weighting curves showing the relative importance of the various section angles of attack for specified flight conditions are included as an aid in the interpretation of the results.

The calculations indicated that the use of a smooth conventional section will result in marked performance gains throughout the flight range. Definite, though smaller, additional gains in take-off weight and in range and endurance may be realized by the use of a low-drag section. At high forward speeds or at moderate forward speeds and high loadings, however, losses are indicated for the low-drag sections in contrast with the smooth conventional sections. It is demonstrated that, if these losses are to be avoided, the low-drag sections must be designed to avoid the extreme rise in drag coefficient at the higher angles of attack which is characteristic of the low-drag sections now available for use in helicopters.

INTRODUCTION

It is generally recognized that an important part of the power required to operate a helicopter is absorbed by the profile drag of the blade elements; consequently, considerable interest has been shown in the possibility of using laminar-flow, or low-drag, airfoil sections in helicopter rotors. A recent report (reference 1) described the characteristics of several low-drag sections that were developed especially for use in helicopters. Previous low-drag sections had either excessive pitching-moment coefficients or low drag only at extremely low lift coefficients. The sections of reference 1 were designed to give the maximum lift-drag ratio $(L/D)_{max}$ obtainable with zero pitching-moment coefficient, over an appropriate range of Reynolds number.

In order to indicate the magnitude of the performance gains that might result from the use of the new sections and to provide a guide for the development of additional sections, an analysis has been made for several conditions of flight for a helicopter of assumed characteristics. The method of analysis used for hovering flight differs considerably from that used for forward flight. The results for the two flight conditions accordingly are presented separately. Material that is not essential to the analysis but provides substantial aid in understanding the results has been incorporated in an appendix.

SYMBOLS

R rotor-blade radius

b number of blades

c blade chord

r radius of blade element

$x = \frac{r}{R}$

θ pitch angle of blade element

θ_1 difference between hub and tip pitch angles (positive when tip angle is greater)

[redacted]

θ_{75} blade pitch angle at $x = 0.75$

Ω rotor angular velocity, radians per second

V forward speed

μ tip-speed ratio $\left(V \frac{\cos \alpha}{\Omega R}\right)$

α angle of attack of rotor disk

$\lambda \Omega R$ speed of axial flow through rotor disk (positive upward)

α_o section angle of attack (absolute)

c_{d_o} section profile-drag coefficient

c_l section lift coefficient

a slope of lift coefficient against section angle of attack (radian measure)

σ solidity; ratio of total blade area to swept-disk area $(bc/\pi R)$

T rotor thrust

C_T thrust coefficient $\left(\frac{T}{\rho \Omega^2 \pi R^4}\right)$

C_Q torque coefficient $\left(\frac{\text{Rotor torque}}{\rho \Omega^2 \pi R^5}\right)$

P power

C_P power coefficient $\left(\frac{\text{Rotor-shaft power input}}{\rho \Omega^3 \pi R^5}\right)$

C_L lift coefficient $\left(\frac{\text{Rotor lift}}{\frac{1}{2}\rho V^2 \pi R^2}\right)$

α_r angle of attack of blade element from zero lift

α_R angle of attack of blade element at tip

$u_T \Omega R$ velocity component at blade element perpendicular to blade span and parallel to rotor disk

$u_P \Omega R$ velocity component at blade element perpendicular to blade span and to $u_T \Omega R$

[redacted]

$\varphi = \tan^{-1} \frac{u_P}{u_T}$

ψ blade azimuth angle measured from down wind in direction of rotation

W gross weight, pounds

W/S rotor disk loading, pounds per square foot

f parasite-drag area, square feet

ρ air density

Subscripts:

i induced

o profile

HOVERING FLIGHT

In order to indicate the effect of variation in airfoil section drag characteristics on the useful load that can be carried, the rotor thrust developed by a fixed shaft power was calculated for an assumed helicopter rotor in which three different types of airfoil section were successively used. The calculations were, in each case, carried out for a series of blade pitch settings.

Sample Helicopter Rotor

The sample helicopter was assumed to be in hovering flight at sea level. The rotor characteristics were taken to be as follows:

Rotor radius, feet	20
Solidity	0.07
Blade plan form	Rectangular
Blade twist	None
Power available at rotor, horsepower	260

[redacted]

Airfoil Section Characteristics

The NACA 3-H-13.5 section was chosen as representative of the new low-drag sections of reference 1. The NACA 23015 section, for which data are also given in reference 1, was included to permit comparison with a smooth conventional section. In order to permit comparison with a conventional section in a condition believed to be typical of present-day rotors, a "rough" conventional section was included; the drag curve for this section is a composite of data from various sources.

The curves of profile-drag coefficient against angle of attack used for the three sections are shown in figure 1. These curves are representative of Reynolds numbers corresponding to the outer part of the rotor disk, in which most of the profile-drag losses occur. As is shown in the appendix the Reynolds number, Mach number, and angles of yaw encountered by the rotor blade vary considerably over the rotor disk. No attempt was made to modify the curves of figure 1 to allow for these variations; the analysis is thus a comparison of drag curves representative of certain types of airfoil section rather than of specific sections.

The profile-drag values available for high angles of attack were incomplete, especially for the NACA 3-H-13.5 section. The drag data of reference 1 reach an angle of attack of 15° for the NACA 23015 section and of 10° for the NACA 3-H-13.5 section. The following relation, which is based largely on a composite of all the data for high angles of attack of reference 1, was used to extend these data as necessary:

$$\Delta c_{d_o} = 0.25 \, (c_l' - c_l)$$

where

Δc_{d_o} increment in profile-drag coefficient above value at upper end of straight-line portion of lift curve

c_l' lift coefficient as given by extension of straight-line portion of lift curve

This method gives results that agree with the available values for high angles of attack for the low-drag sections of reference 1 within about ±20 percent. It is also in

[redacted]

approximate agreement with drag data for other airfoils at angles of attack beyond the stall.

The slope of the airfoil section lift curve was taken as 5.85 throughout the analysis.

Method of Calculation of Thrust for Fixed Horsepower

Thrust.- The rotor thrust T is

$$T = C_T \rho \pi R^4 \Omega^2$$

or, for the assumed rotor,

$$T = 1195 C_T \Omega^2 \tag{1}$$

The value of C_T for a given blade pitch setting may be obtained from equation (14) of reference 2, which may be written

$$C_T = \sigma^2 a \left\{ \frac{\theta}{6\sigma} + \frac{1}{8}\frac{a}{8} - \frac{\sigma^2}{32\theta^2\left(\frac{a}{8}\right)^2}\left[\frac{A^5}{5} - \left(\frac{a}{8}\right)^2 \frac{A^3}{3} + \frac{2}{15}\frac{a}{8}\right]\right\}$$

where

$$A = \sqrt{\left(\frac{a}{8}\right)^2 + 4\frac{a}{8}\frac{\theta}{\sigma}}$$

In order to obtain an expression for Ω, the power required and the power available may be equated as

$$P = 260 \text{ hp} = \rho \pi R^5 \Omega^2 C_{Q_i} \frac{\Omega}{550} + \rho \pi R^5 \Omega^2 C_{Q_o} \frac{\Omega}{550}$$

hence,

$$\Omega = \sqrt[3]{\frac{260}{43.46\left(C_{Q_i} + C_{Q_o}\right)}} \tag{2}$$

Induced torque coefficient.- The value of C_{Q_i} for a given pitch setting may be obtained by using the

[redacted]

figure-of-merit equation of reference 2, which may be written

$$M = 0.707\frac{C_T^{3/2}}{C_Q}$$

hence,

$$C_{Q_i} = 0.707\frac{C_T^{3/2}}{M_i}$$

Values of M_i for any specified value of pitch may be obtained from figure 17 of reference 2. The factor in the above equation is 0.707 instead of 1/2 as in reference 2 since $\rho/2$ was used in the definition of C_T and C_Q in reference 2, whereas ρ is used in the definitions throughout the present report.

Profile torque coefficient.- In order to obtain the desired values of C_{Q_o} for a drag curve of arbitrary form, it is necessary first to calculate the induced angle of flow at a series of radii for each of the specified pitch angles. This calculation was made by means of equation (11) of reference 2, which may be written

$$\varphi = \frac{\sigma}{2x}\left[\frac{a}{8} - \sqrt{\left(\frac{a}{8}\right)^2 + 4\frac{a}{8}\frac{\theta x}{\sigma}}\right]$$

where an upward inclination of the flow is associated with positive values of φ; hence,

$$\varphi = \frac{0.035}{x}\left(0.731 - \sqrt{0.534 + 41.88x}\right)$$

The angles of attack are then obtained from the relation

$$\alpha_r = \theta + \varphi$$

Sample curves of angle of attack against fraction of radius are shown in figure 2.

[redacted]

The torque coefficient per foot of radius can then be obtained from the expression $\frac{bc\,c_{d_o}x^2}{2\pi R^2}$. The torque coefficient for the entire rotor is then readily obtained by graphical integration.

After both C_{Q_i} and C_{Q_o} are obtained, equation (2) may be solved for Ω and equation (1) may then be solved for T.

Results of Hovering Analysis

Rotor thrust was calculated for a range of pitch angle from 7° to 21°. The results are shown in figure 3. Curves for zero profile drag and for the still more ideal case of zero profile drag together with uniform induced velocity have been included for comparison. The maximum section angle of attack, that is, at the blade tip, is indicated in figure 3 along with the blade pitch. At the higher pitch angles, the slope of the airfoil lift curves falls off and the calculated thrust values are optimistic. These portions of the curves have been drawn as dashed lines.

Discussion of Results of Hovering Analysis

It is apparent from figure 3 that, within the range of tip speed corresponding to present practice, the relative merit of the three sections being considered remains virtually fixed. A change from the rough conventional section to the smooth NACA 23015 section results in an increase in rotor thrust of more than 300 pounds. Changing from the smooth NACA 23015 section to the smooth NACA 3-H-13.5 section results in a further increase of approximately 200 pounds. It is noteworthy that only about 300 pounds more could be gained if the profile drag could be made zero.

The calculated values of maximum available thrust shown in figure 3 are greater than the gross weight assumed in the forward-flight analysis. The lower gross weight was assumed because, in a practicable machine, the ability to hover at altitude and the ability to take off with an overload are considered desirable features.

[redacted]

FORWARD FLIGHT

Of the various performance characteristics associated with forward flight, range and endurance seem of greatest interest at the present time. Calculations of range and endurance at a particular airspeed (approximately that for minimum power) consequently were made for a sample helicopter in which the three airfoil sections previously described were used successively. A fuel load of 10 percent of the gross weight was assumed in each case. The power absorbed by all items other than the rotor, including cooling fans and torque-compensating devices, was allowed for by assuming a specific fuel consumption of 0.55 pound per rotor horsepower-hour, which is approximately 15 to 20 percent higher than the normal value for cruising power.

Because of the irregular shape of the drag curve for the low-drag airfoil, analytical treatments of the rotor profile-drag losses, such as that of reference 3, were not feasible and graphical methods were used.

Sample Helicopter and Assumed Conditions

The sample helicopter was assumed to be in level flight at sea level and to be operating under the following conditions:

Forward speed	
Feet per second	80
Miles per hour	55
Rotor tip speed, feet per second	400
Tip-speed ratio	0.2

The geometric characteristics assumed were as follows:

Rotor radius, feet	20
Disk loading, pounds per square foot	2.5
Gross weight, pounds	3140
Blade plan form	Rectangular
Blade twist	None
Solidity	0.07
Parasite-drag area, square feet	15

[redacted]

Except where otherwise indicated, the foregoing assumptions apply to all results presented for forward flight. It will be noted that the geometric characteristics assumed for the rotor are the same as those used in the hovering analysis.

Method of Analysis

The power absorbed by the rotor may be considered as the sum of the power required to overcome the parasite drag, the induced drag, and the rotor-blade profile drag. The power required to overcome the parasite drag is

$$P_p = \frac{1}{2}\rho V^2 f \frac{V}{550}$$

$$= 16.6 \text{ horsepower}$$

which is considered to be constant. The horsepower required to overcome the induced drag is

$$P_i = \left(\frac{D}{L}\right)_i W \frac{V}{550}$$

As explained in reference 3, the induced D/L is simply $C_L/4$. Because the change in weight is small, the use of the average weight is considered permissible, and the average induced power is then

$$P_i = 0.0783 \times 2980 \times \frac{80}{550}$$

$$= 33.9 \text{ horsepower}$$

The calculation of profile-drag losses is much more complex and is described in some detail.

Calculation of angles of attack.- Any graphical treatment of profile-drag losses requires knowledge of blade section angle of attack at various points on the rotor disk. In order to calculate the angle of attack of a blade element at any given point, it is necessary first to calculate the required blade pitch, the inflow velocity, and the blade flapping coefficients. The pitch and the inflow velocity were determined by means of the analysis described in reference 4. This analysis

[redacted]

extends the analysis of reference 3 by the addition of a parameter that represents the shaft power supplied to the rotor. The flapping coefficients were then determined by equations (1) to (5) of reference 3.

In determining the pitch and inflow velocity, it was necessary to estimate the rotor profile-drag losses. This estimation was accomplished by use of a specific airfoil drag curve as represented by a power series. The drag curve used corresponds to that employed in the example of reference 3, but the resulting values of rotor profile drag were decreased about 10 percent to provide a better approximation to the characteristics of the smooth sections being considered in the present study. In a strict sense, a different combination of pitch and inflow velocity should be determined for each section, particularly for the rough conventional section, because of the difference in required power input; however, the effects of such changes in the combination of pitch and inflow velocity are negligible except in cases in which the retreating tip-section angles become high enough to produce excessive drag. The effect of an extreme change in power input and in the resulting combination of pitch and inflow velocity may be noted by referring to the example given in the appendix; this example compares the rotor profile-drag losses when 15 square feet of parasite-drag area and zero parasite-drag area are successively assumed at a relatively high forward speed.

The normal and tangential components of velocity relative to a blade element were obtained from the following expressions, which are modifications of equations (8) and (9) of reference 5:

$$u_T = K_1 + x$$

$$u_P = K_2 + K_3 x$$

where

$$K_1 = \mu \sin \psi$$

$$K_2 = \lambda + \frac{1}{2}\mu a_1 + \left(-\mu a_0 + \frac{1}{2}\mu a_2\right) \cos \psi + \frac{1}{2}\mu b_2 \sin \psi + \frac{1}{2}\mu a_1 \cos 2\psi + \frac{1}{2}\mu b_1 \sin 2\psi + \frac{1}{2}\mu a_2 \cos 3\psi + \frac{1}{2}\mu b_2 \sin 3\psi$$

[redacted]

$K_3 = b_1 \cos \psi - a_1 \sin \psi + 2b_2 \cos 2\psi - 2a_2 \sin 2\psi$

and a_o, a_1, a_2, b_1, and b_2 represent coefficients in the Fourier series expressing the blade flapping motion.

In reference 6 the angle of attack of an element α_r is shown to be equal to $\theta + \tan^{-1} \frac{u_P}{u_T}$. In the present analysis, the tangent was assumed equal to the angle in radians; hence, the angle in degrees is

$$\alpha_r = 57.3\left(\theta + \frac{u_P}{u_T}\right)$$

Values of α_r were calculated at every 10° azimuth and at intervals of 0.1R over the blade radius, so that values were provided at a total of 360 points on the rotor disk.

Profile-drag power loss.- The rate of profile-drag energy dissipation for a blade element of unit length is the product of the drag and the relative velocity, or

$$P_o = \frac{1}{2}\rho\left(\frac{u_T \Omega R}{\cos \varphi}\right)^2 bc\, c_{d_o} \frac{u_T \Omega R}{\cos \varphi}$$

For the conditions of operation covered by the present analysis, a negligible error is introduced by the omission of $\cos \varphi$ and the profile-drag power loss per foot of radius becomes

$$P_o = \frac{1}{2}\rho(u_T \Omega R)^3 bc\, c_{d_o}$$

By using the assumed values of solidity, blade radius, and tip speed, there is obtained in foot-pounds per second per foot of radius

$$P_o = 334{,}000 u_T^3 c_{d_o} \qquad (3)$$

In order to obtain the total power for a given airfoil, the drag coefficient corresponding to the calculated angle of attack at each point in the disk is used successively in equation (3). The details of the integration of the 360 values are omitted.

[redacted]

In order to obtain curves of profile-drag power loss against weight, calculations of angle of attack and energy loss were carried out for five values of gross weight. The resulting curves are shown in figure 4. The values for the rough airfoil obtained analytically are included for comparison with the values obtained graphically. In order to permit such calculations, the drag curve of figure 1 for the rough airfoil was made to have, up to an angle of attack of 10°, the same form as that of the example given in reference 3; the ordinates were, however, increased 28 percent in order to make the desired allowance for surface roughness. Values of D/L obtained as described in reference 3 could thus be used after being increased 28 percent.

Calculation of Range and Endurance

By using the average profile-drag loss in horsepower, as given by figure 4, for the range of weight from 3140 pounds to 2830 pounds, the average total rotor drag losses for each airfoil section may be evaluated as follows:

Drag losses (hp) \ Airfoil	Rough conventional	Smooth NACA 23015	Smooth NACA 3-H-13.5
Parasite	16.6	16.6	16.6
Induced	33.9	33.9	33.9
Profile	47.3	27.3	20.0
Total	97.8	77.8	70.5

By assuming a specific fuel consumption of 0.55 pound per rotor horsepower-hour, the values of range and endurance are as follows:

Airfoil	Rough conventional	Smooth NACA 23015	Smooth NACA 3-H-13.5
Range, miles	320	400	440
Endurance, hours	5.8	7.3	8.1

[redacted]

High-Speed Condition

As an indication of the effect of tip-speed ratio on the relative merit of the airfoil sections, calculations were made for the sample helicopter at a tip-speed ratio of 0.3. The corresponding forward speed becomes 120 feet per second, or about 80 miles per hour; all other assumptions are as previously given. The drag losses then are as follows:

Drag losses (hp) \ Airfoil	Rough conventional	Smooth NACA 23015	Smooth NACA 3-H-13.5
Parasite	56.0	56.0	56.0
Induced	25.0	25.0	25.0
Profile	67.5	33.5	54.5
Total	148.5	114.5	135.5

The high profile-drag loss for the low-drag section results from the high drag values above the low-drag notch; this point is demonstrated in the appendix.

Discussion of Results of Forward-Flight Analysis

It is apparent from figure 4 that the relative merit of the airfoils depends on the loading used. Certain aspects of the comparison are brought out more clearly by plotting the profile drag-lift ratio $(D/L)_o$ instead of power loss. Figure 5 shows this factor plotted against the loading factor $2C_T/\sigma a$, which is more general than but is proportional to weight or loading. It is evident that the optimum $(D/L)_o$ occurs at a considerably lower loading for the NACA 3-H-13.5 section than for the NACA 23015 section.

Although a relatively small portion of the rotor disk is affected, it should be pointed out that the assumption of constant lift-curve slope is not strictly valid at the high loadings and at $\mu = 0.3$. The calculations for the NACA 3-H-13.5 section, in particular, are increasingly optimistic as these conditions are reached.

[redacted]

CONCLUSIONS

The effect of modifications in the airfoil section drag characteristics, as indicated by the theoretical performance analysis made for the sample helicopter, may be summarized as follows:

1. The use of the section characteristics taken as representative of a smooth conventional section instead of those taken as representative of a rough conventional section resulted in an increase of approximately 9 percent in the rotor thrust available with fixed shaft power in hovering, an increase of 25 percent in range and endurance (with equal fuel load) at cruising speed, and a reduction of 23 percent in the power required at a relatively high forward speed (80 mph; tip-speed ratio, 0.3).

2. The use of the section characteristics taken as representative of the low-drag airfoils of NACA CB No. 3I13 instead of those for the smooth conventional section resulted in a further increase of approximately 5 percent in the rotor thrust available with fixed shaft power in hovering and an additional increase of 10 percent in range and endurance at cruising speed; however, at the high-speed condition, an increase of approximately 18 percent in the power required was indicated.

3. If the losses shown for the low-drag section at high speeds and at moderate speeds and high loadings are to be avoided, the low-drag section must be designed to prevent the extreme rise in drag coefficient at the higher angles of attack exhibited by the low-drag sections of NACA CB No. 3I13.

Langley Memorial Aeronautical Laboratory
National Advisory Committee for Aeronautics
Langley Field, Va.

[redacted]

APPENDIX

CONDITIONS OF OPERATION ENCOUNTERED BY THE BLADE SECTION AND EFFECT OF VARIATIONS IN ASSUMPTIONS

Contours of angle of attack and power loss.- In order to make the reason for the results obtained in the forward-flight analysis more evident, contours of angle of attack and power loss were prepared. The source of the values of section angle of attack has already been sufficiently explained. In order to show the relative importance of a given increment in drag coefficient in the different parts of the rotor disk, the expression previously given for power loss per foot of radius was modified by dividing by the area of the annulus at the appropriate radius; the resulting expression for the power loss in foot-pounds per second per square foot of disk area for a profile-drag coefficient of 0.01 is

$$P_o = 26.60 \frac{u_T^3}{x}$$

Contours for the set of conditions initially assumed are shown in figure 6(a). Figure 6(b) shows the effect on the contours of increasing the assumed value of solidity. Changes in loading produce similar effects, since the higher solidity is comparable with lower loading. Contours for the original solidity but for $\mu = 0.3$ ($V \approx 80$ mph) instead of $\mu = 0.2$ ($V = 55$ mph) are shown in figure 7.

Weighting curves.- The contours in figures 6 and 7 indicate that a given increment of profile-drag coefficient is more important at low than at high section angles of attack. It is difficult, however, to judge the significance of certain factors - for example, the abrupt rise in drag coefficient at high angles of attack shown for the NACA 3-H-13.5 section (fig. 1). In order to permit more rapid quantitative judgement of such factors, the data may be combined for the two sets of contours into a single curve showing the relative importance of different parts of the curve of airfoil section profile-drag coefficient against section angle of attack. This weighting curve is designed to show the amount by

which the power consumed in overcoming the profile drag of all the blade elements operating at any particular angle of attack is increased if the airfoil section drag coefficient corresponding to that angle of attack is increased by some convenient increment, for example, 0.01. Such a curve has the further merit of permitting rapid calculation of total power for any airfoil section; it is necessary only to multiply the ordinates of the curve of profile-drag coefficient against angle of attack characteristic of the airfoil section by the ordinates of the weighting curve and obtain the area under the resulting curve.

In order to obtain such a weighting curve, the range (or ranges) of azimuth angle (ψ_1 to ψ_2) through which a given range of angle of attack (α_{r_1} to α_{r_2}) was maintained was determined for a given radius by using a plot of angle of attack against azimuth angle for that radius. The process was repeated for successive ranges of angle of attack until the entire circumference was accounted for. The appropriate average value of u_T^3 for each range of azimuth angle was then read from a plot of u_T^3 against azimuth angle. Ordinates for the weighting curve for the specified radius were then obtained by means of the expression for the energy per second per degree angle of attack per foot of radius

$$\frac{1}{2}\rho bc\, c_{d_o}\overline{u_T^3}\Omega^3 R^3 \frac{\psi_2 - \psi_1}{360}\frac{1}{\alpha_{r_2} - \alpha_{r_1}}$$

where $\overline{u_T^3}$ is the average value of u_T^3 for the range from ψ_1 to ψ_2. It was found that increments of angle of attack of 0.2° provided ample detail in the final curve.

The process was repeated at intervals of 0.1R over the blade radius. The resulting weighting curves for representative radii and the over-all weighting curve obtained by a summation of the curves at the various radii are shown in figure 8 for $\mu = 0.2$. Values of power obtained by use of the curve of figure 8 and other values obtained from each of a number of other weighting curves were checked against corresponding values obtained by the more laborious point-by-point method already described, and the answers agree within ± 0.3 horsepower.

[redacted]

In order to permit ready application of the weighting curves to rotors differing from the sample rotor in chord, radius, or airfoil section and likewise to rotors operating at different tip speeds and altitudes, the curves have been plotted in nondimensional form. The use of the curves for calculation of the profile-drag loss for a particular rotor and a particular airfoil section involves the following steps:

(1) Multiply the ordinates of the weighting curve by the ordinates of the curve for airfoil section profile-drag coefficient

(2) Multiply the resulting ordinates by 100 to allow for the fact that the weighting-curve ordinates were given for $c_{d_o} = 0.01$

(3) Obtain the area under the resulting curve and thus obtain the total value of C_p/σ

(4) Multiply the value of C_p/σ by the factor

$$\sigma \frac{\rho \Omega^3 \pi R^5}{550}$$

Steps (2) and (4) may of course be combined; the factor for the sample rotor is then

$$\frac{100 \times 0.07 \times 0.002378 \times (20)^3 \times \pi \times (20)^5}{550} = 2.43 \times 10^6$$

Effect of variations in helicopter characteristics and flight conditions.- The weighting curves provide a convenient means for indicating the effect of changes in assumptions on the airfoil requirements. The effects of tip-speed ratio, loading, solidity, blade twist, and power input are thus indicated in figure 9. Corresponding profile-drag losses for the drag curves under consideration are given in table I.

Source of losses indicated for low-drag airfoil.- Comparison of the weighting curves of figure 9 with the profile-drag curves of figure 1 shows that, for the conditions in which the low-drag airfoil shows losses instead of gains, these losses result from the extremely high values of profile-drag coefficient at the high angles

[redacted]

of attack. The point is brought out more clearly in figure 10, which shows the curves that result from multiplying the drag curves of figure 1 by the corresponding weighting curves of figure 9(a) for $\mu = 0.3$.

Preliminary results (unpublished) of additional low-drag airfoils intended to reduce these losses at high angles of attack indicate that considerable progress may be expected.

Conditions of operation ignored in analysis.- Simplifying assumptions or procedures, which have been used in the analysis but have not been discussed and may be suspected of endangering the validity of the comparisons made, include:

(1) Use of statically measured section characteristics with no allowance for effects due to rotation

(2) Assumption of uniform inflow velocity (forward-flight analysis only)

(3) Use of section characteristics corresponding to a single Reynolds number and a single Mach number as applying at all points on the rotor disk

(4) Neglect of effect of angles of yaw on section characteristics

Past experience indicates that airfoil sections used in rotating blades exhibit characteristics similar to their statically measured section characteristics. Possible effects on the characteristics of the low-drag sections are conjectural.

The effect of nonuniformity of inflow velocity was examined in reference 6, and it was concluded that the net effect on the rotor forces was secondary.

The method of analysis used would permit study of items (3) and (4), or even inclusion of the effects in the analysis if such were deemed desirable and if sufficient section data were available. Although the data at hand are insufficient to permit complete calculations, it is of interest to note the magnitude of the variations of Reynolds number, Mach number, and angle of yaw.

[redacted]

The Reynolds number, which was taken as approximately 3×10^6 in choosing the drag curves, actually varies from 0 to 4.5×10^6 in a typical case. The value 2.8×10^6 corresponds to the mean value at $x = 0.75$ when the number of blades is taken as three. Figure 11 shows the variation of Reynolds number over the rotor disk for two tip-speed ratios. Radial components of velocity are ignored. Comparison with figures 6 and 7 indicates the regions in which the greatest differences might result if the drag curves were varied with Reynolds number.

The contours of figure 11 may also be used in estimating Mach numbers. For this purpose, the values shown on the contours should be multiplied by $0.000014\Omega R$. For the sample rotor in forward flight, $\Omega R = 400$; hence, the Mach number is approximately equal to the value shown on the appropriate contour line times 0.0056. For $\mu = 0.2$, the maximum tip Mach number is thus 0.42 at $\psi = 90°$ and the minimum is 0.28 at $\psi = 270°$.

The variation of angle of yaw over the rotor disk at a tip-speed ratio of 0.2 is shown in figure 12. The same contours can also be applied to any value of μ above 0.2 by placing a new outer boundary at a radius equal to $0.2/\mu$ times the original radius; the tip circle for $\mu = 0.4$ has been drawn in as an example. It is of interest to note that the regions which appear in figures 6 and 7 to be the most critical - that is, the region of high power loss per unit drag coefficient on the advancing side and the region in which tip stalling is approached on the retreating side - include relatively low angles of yaw.

[redacted]

REFERENCES

1. Tetervin, Neal: Tests in the NACA Two-Dimensional Low-Turbulence Tunnel of Airfoil Sections Designed to Have Small Pitching Moments and High Lift-Drag Ratios. NACA CB No. 3I13, 1943.

2. Knight, Montgomery, and Hefner, Ralph A.: Static Thrust Analysis of the Lifting Airscrew. NACA TN No. 626, 1937.

3. Bailey, F. J., Jr.: A Simplified Theoretical Method of Determining the Characteristics of a Lifting Rotor in Forward Flight. NACA Rep. No. 716, 1941.

4. Bailey, F. J., Jr., and Gustafson, F. B.: Charts for Estimation of the Characteristics of a Helicopter Rotor in Forward Flight. I - Profile Drag-Lift Ratio for Untwisted Rectangular Blades. NACA ACR No. L4H07, 1944.

5. Wheatley, John B.: An Analytical and Experimental Study of the Effect of Periodic Blade Twist on the Thrust, Torque, and Flapping Motion of an Autogiro Rotor. NACA Rep. No. 591, 1937.

6. Wheatley, John B.: An Aerodynamic Analysis of the Autogiro Rotor with a Comparison between Calculated and Experimental Results. NACA Rep. No. 487, 1934.

[redacted]

TABLE I.- EFFECT OF VARIATIONS IN HELICOPTER CHARACTERISTICS AND FLIGHT CONDITIONS

Figure	Conditions (a)			Profile-drag loss (hp)			
				For $c_{d_o} = 0.01$	For rough conventional section	For smooth NACA 23015 section	For smooth NACA 3-H-13.5 section
Effect of loading (hovering flight)							
	μ (b)	W/S	θ (deg)				
9(a)	0	1.55	7	30.2	33.7	21.4	16.0
	0	3.33	13	30.2	50.5	28.2	14.5
	0	5.42	19	30.2	94.2	42.3	204.6
Effect of tip-speed ratio							
	μ (b)	W/S	θ (deg)				
9(a)	0	2.5	10.3	30.2	40.6	23.9	14.2
	.2	2.5		33.7	49.0	27.8	23.2
	.3	2.5		38.3	67.5	33.5	54.5
Effect of loading							
	μ	W/S					
9(b)	0.2	1.9		33.7	42.3	25.7	18.2
		2.5		33.7	49.0	27.8	23.2
		3.1		33.7	58.8	31.3	54.3

[a] All conditions not specified correspond to original assumptions.

[b] All values given for $\mu = 0$ are for tip speed of 400 fps to permit comparison with values for forward flight.

TABLE I.- EFFECT OF VARIATIONS - Concluded

Figure	Conditions (a)			Profile-drag loss (hp)			
				For $c_{d_o} = 0.01$	For rough conventional section	For smooth NACA 23015 section	For smooth NACA 3-H-13.5 section
Effect of solidity							
	μ	σ					
9(c)	0.2	0.07		33.7	49.0	27.8	23.2
		.10		48.1	59.6	36.2	26.1
Effect of blade twist							
	μ	θ_1 (deg)					
9(d)	0.3	0		38.3	67.5	33.5	54.5
		-8		38.3	54.9	31.1	42.4
Effect of power input							
	μ	θ_1 (deg)	f (sq ft)				
9(e)	0.3	-8	15	38.3	54.9	31.1	42.4
			0	38.3	53.8	30.8	35.9

[a]All conditions not specified correspond to original assumptions.

NATIONAL ADVISORY
COMMITTEE FOR AERONAUTICS

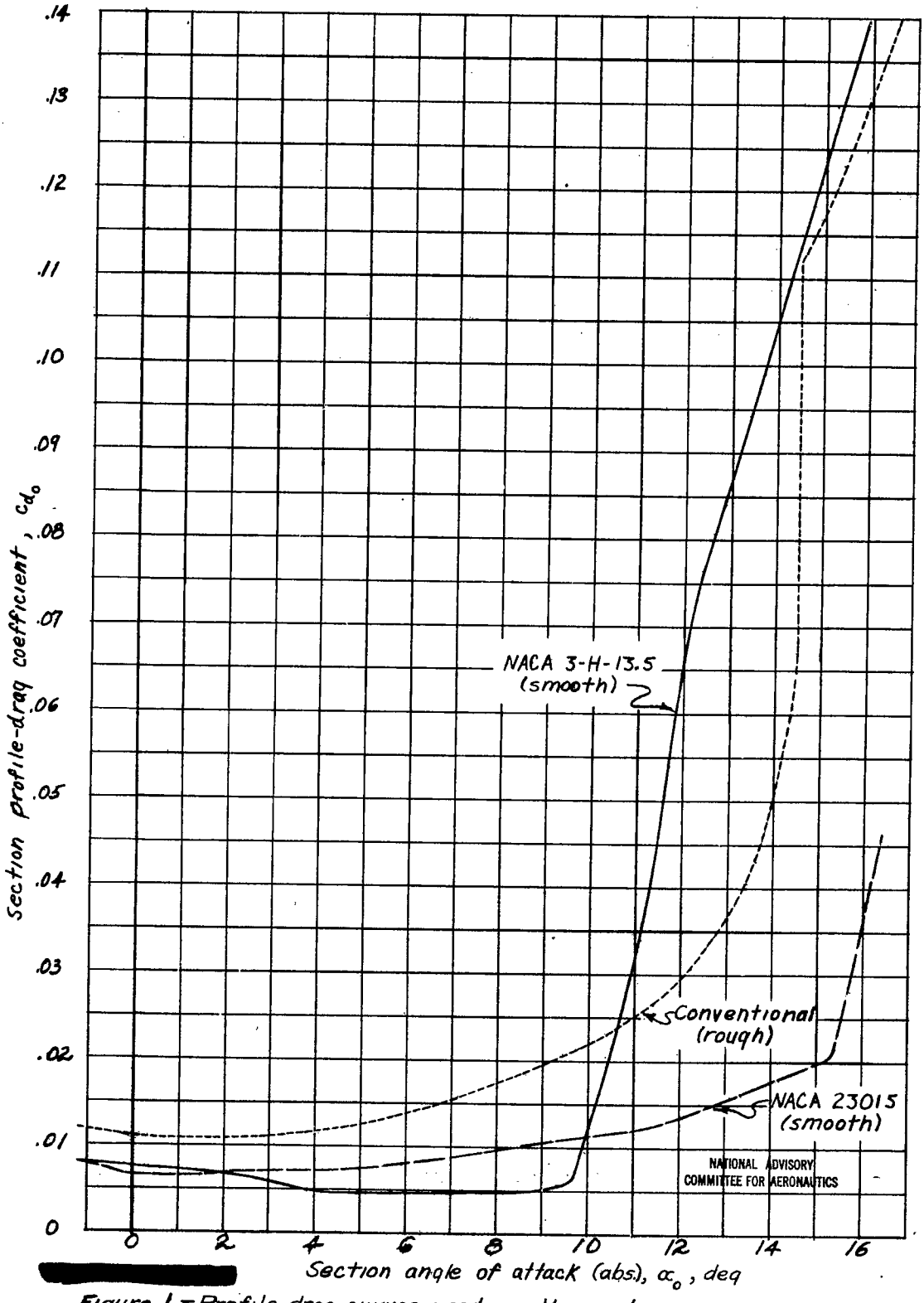

Figure 1.—Profile-drag curves used in the analysis.

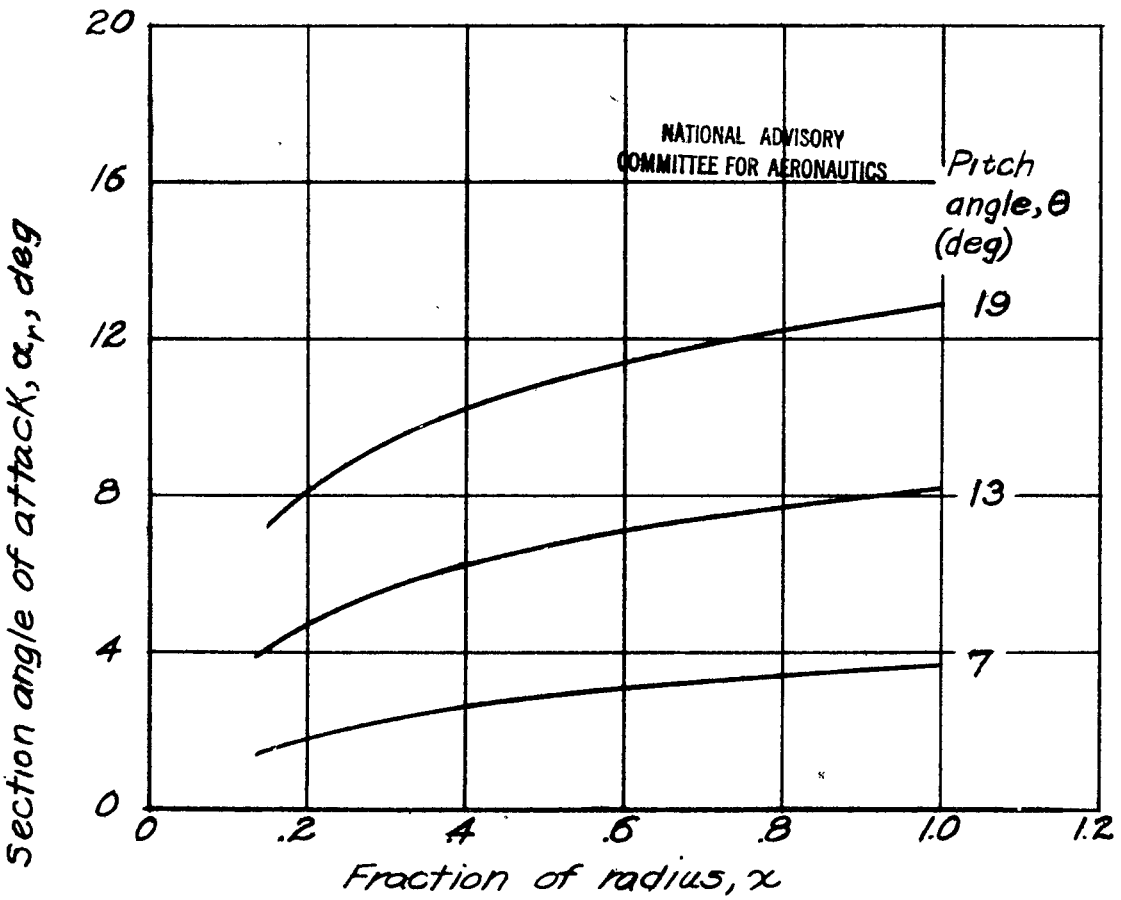

Figure 2.- Section angles of attack for three pitch settings. Sample helicopter rotor in hovering flight.

[redacted]

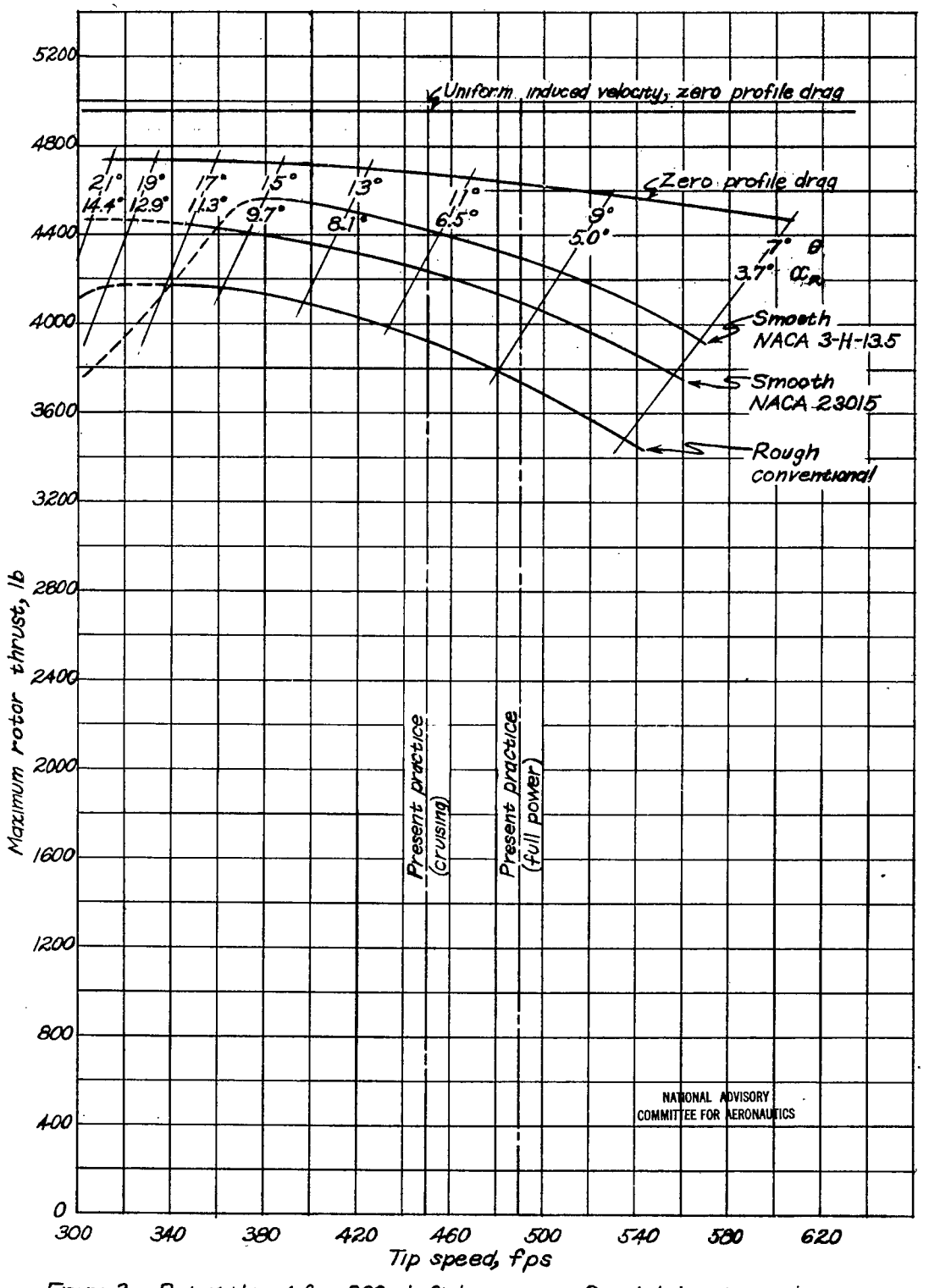

Figure 3.- Rotor thrust for 260 shaft horsepower. Sample helicopter in hovering flight.

[redacted]

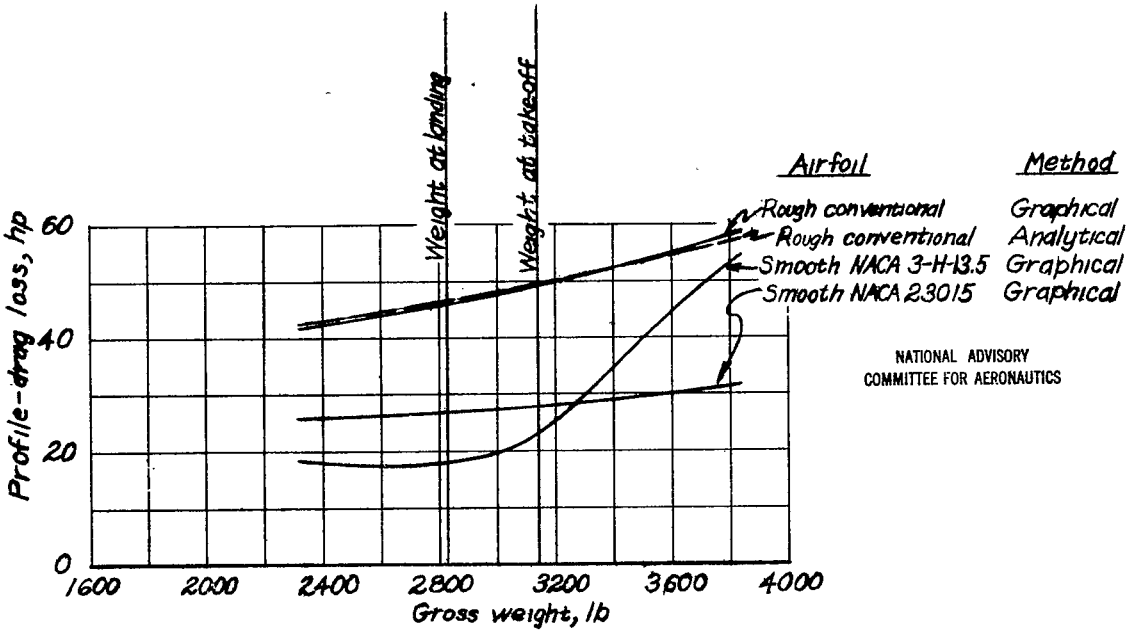

Figure 4.- Rotor profile-drag loss for a range of gross weight. Sample helicopter; μ=0.2.

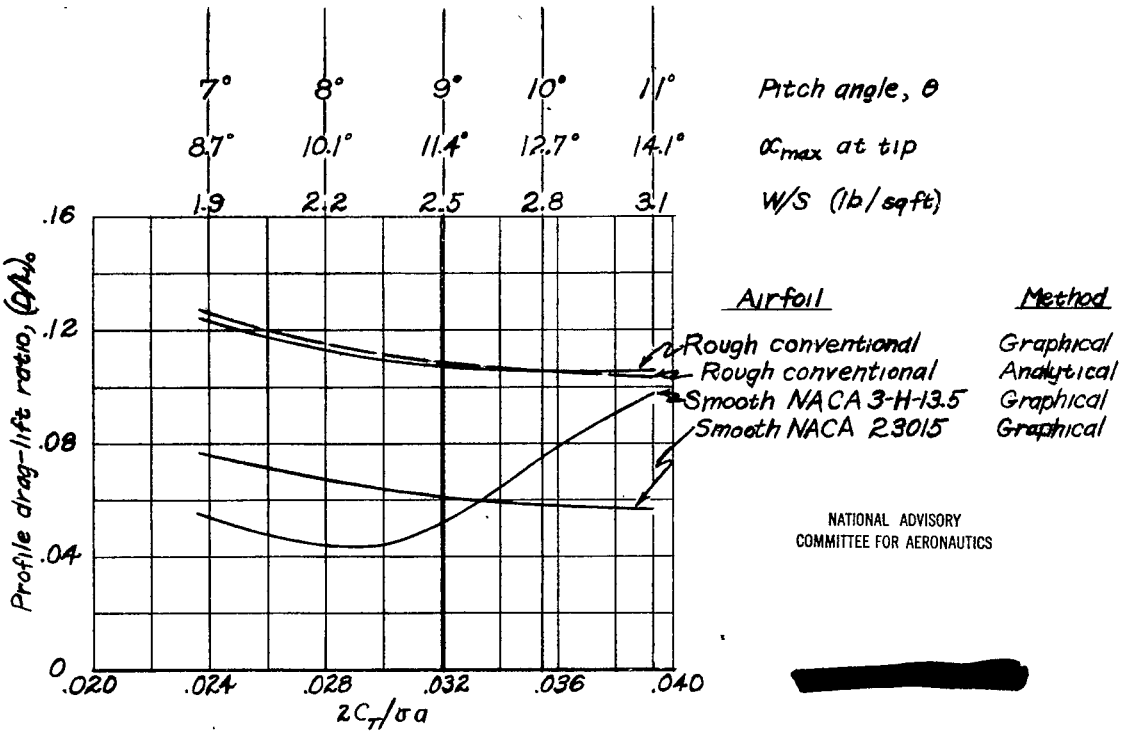

Figure 5.- Rotor profile drag-lift ratio as affected by loading. Sample helicopter rotor; μ=0.2.

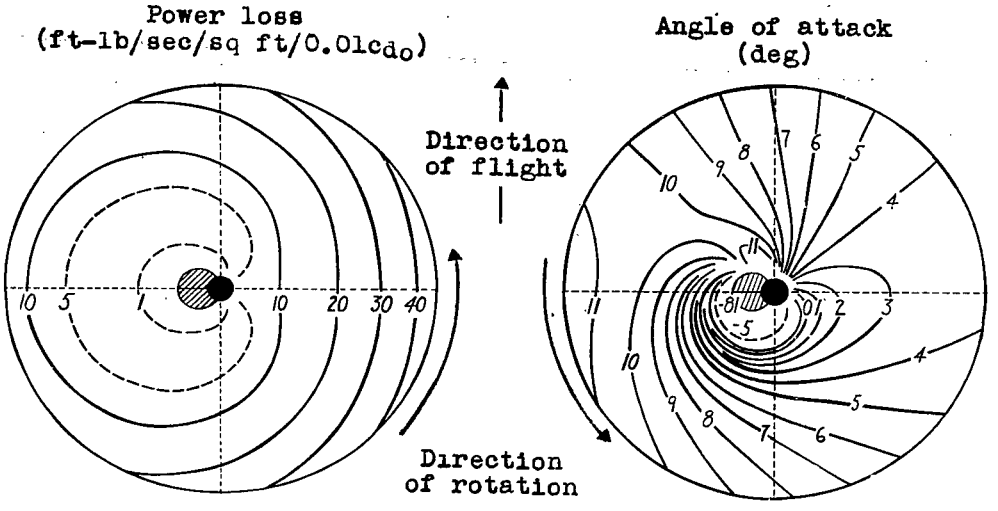

(a) Original solidity; $\lambda = -0.0385$; $\theta = 9^\circ$; $\sigma = 0.07$; $\frac{2C_T}{\sigma a} = 0.0321$.

NATIONAL ADVISORY
COMMITTEE FOR AERONAUTICS

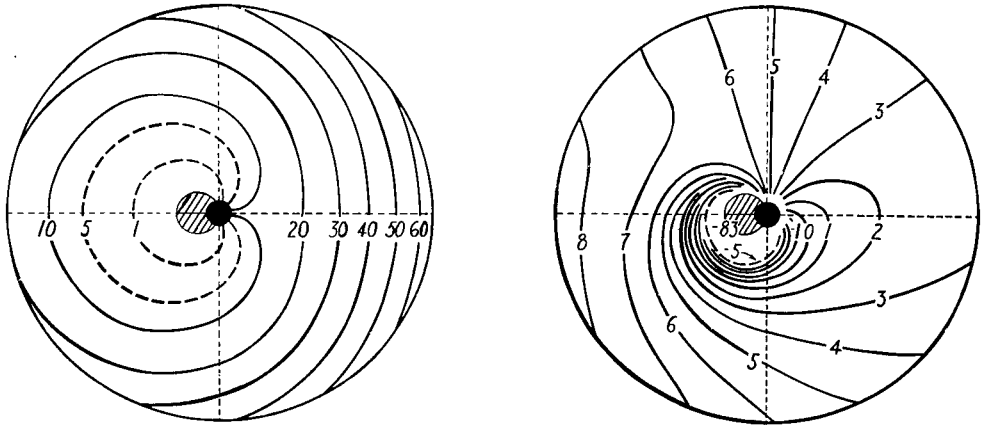

(b) Increased solidity; $\lambda = -0.0350$; $\theta = 7^\circ$; $\sigma = 0.10$; $\frac{2C_T}{\sigma a} = 0.0225$.

Figure 6.- Contours of power loss and angle of attack for sample helicopter rotor and for an alternate rotor with higher solidity and lower pitch. $V = 55$ miles per hour; $\mu = 0.2$; $\frac{W}{S} = 2.5$ pounds per square foot.

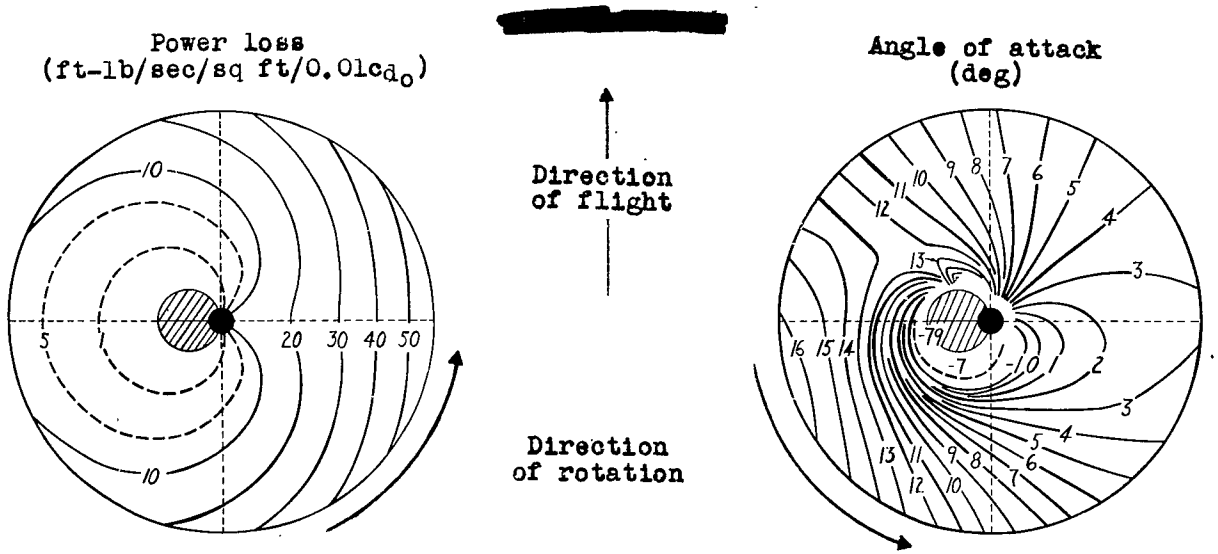

Figure 7.- Contours of power loss and angle of attack for sample helicopter rotor. $V \approx 80$ miles per hour; $\mu = 0.3$; $\frac{W}{S} = 2.5$ pounds per square foot. $\lambda = -0.0695$; $\theta = 11^{\circ}$; $\sigma = 0.07$; $\frac{2C_T}{\sigma a} = 0.0321$.

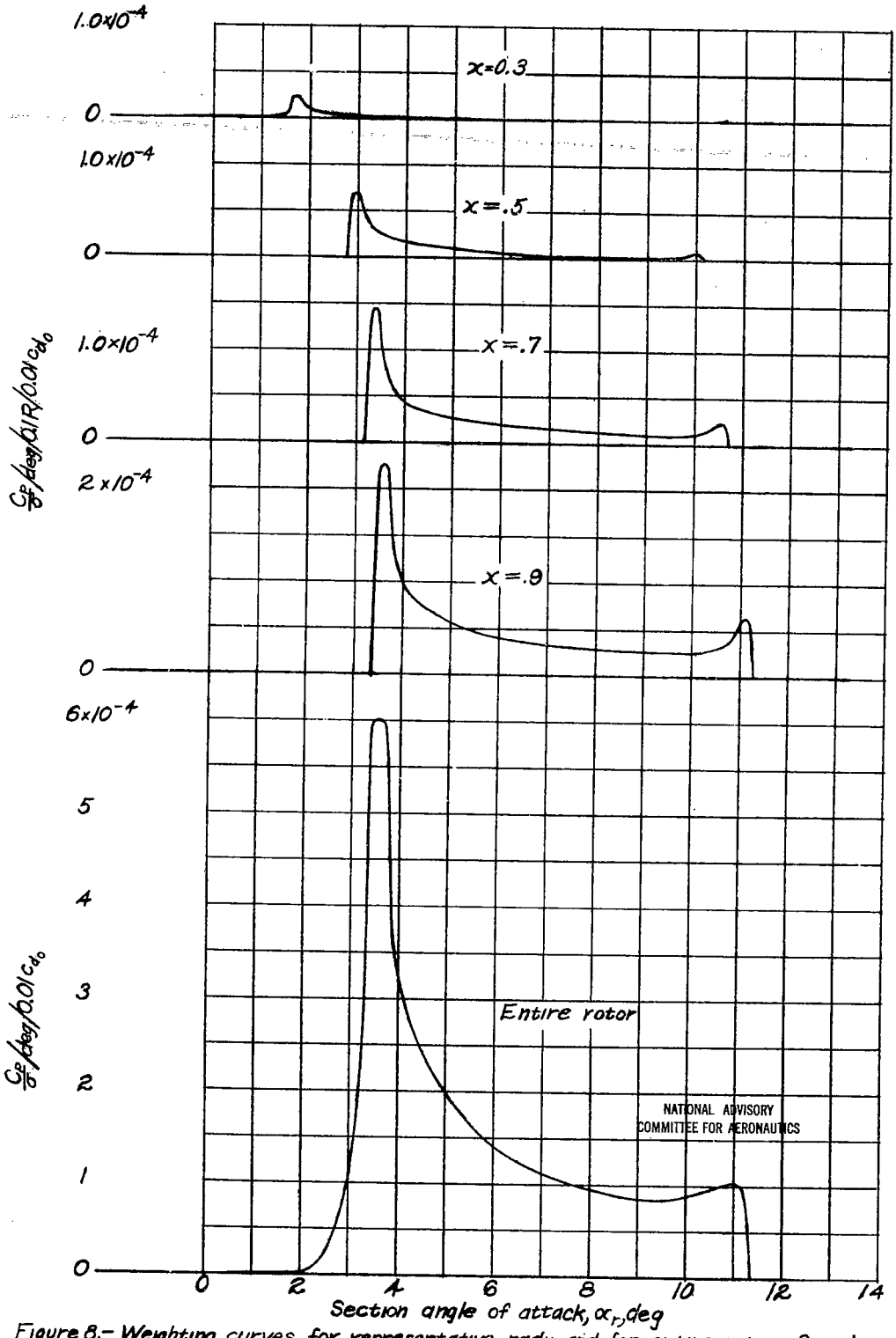

Figure 8.- Weighting curves for representative radii and for entire rotor. Sample helicopter rotor; $\mu=0.2$; $\theta=9°$; $\lambda=-0.0385$.

[redacted]

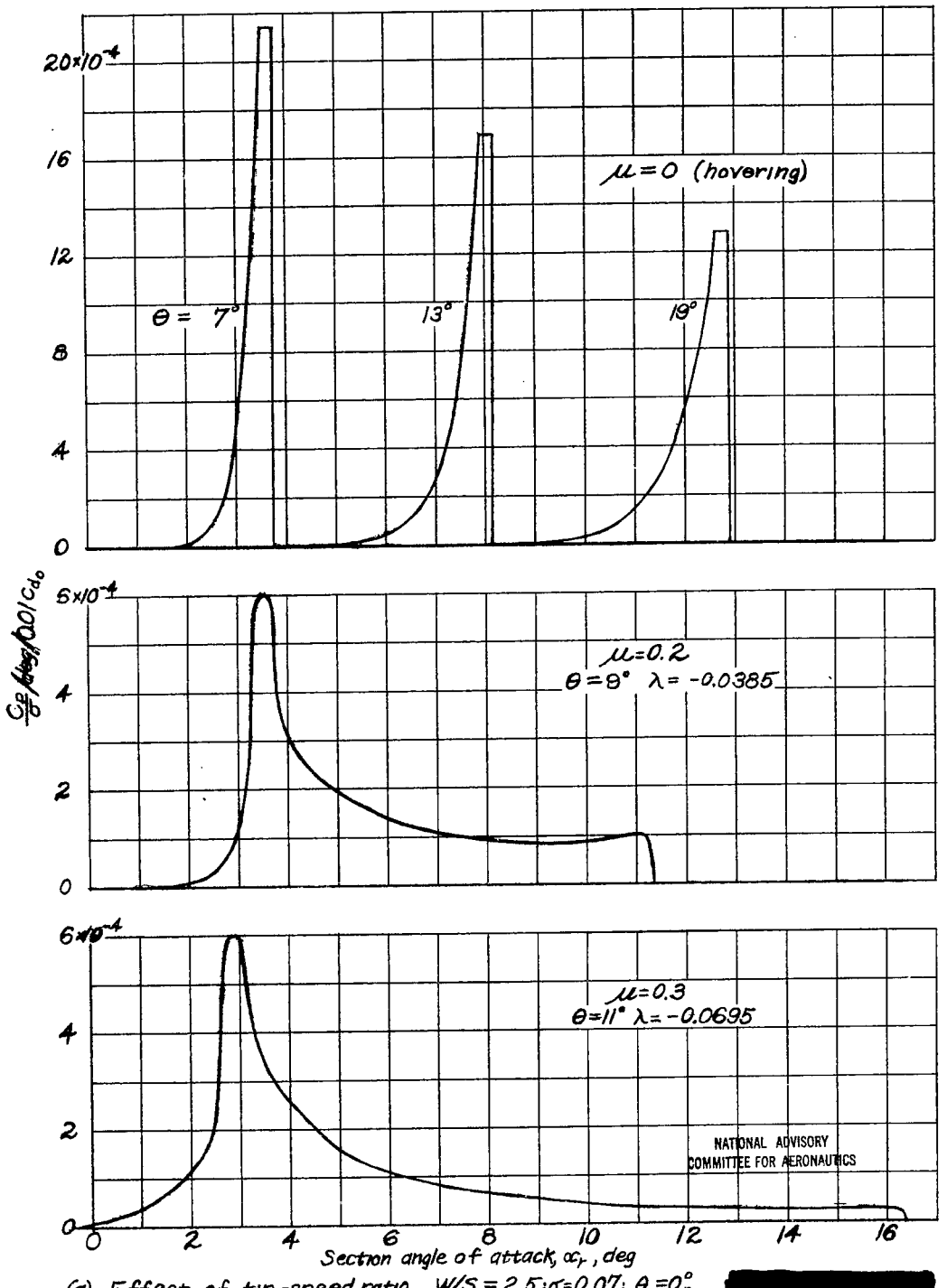

(a) Effect of tip-speed ratio. $W/S = 2.5$; $\sigma = 0.07$; $\theta_1 = 0°$.

Figure 9.- The effect of various changes in the operating conditions and geometric characteristics assumed for the sample rotor, as shown by the corresponding weighting curves.

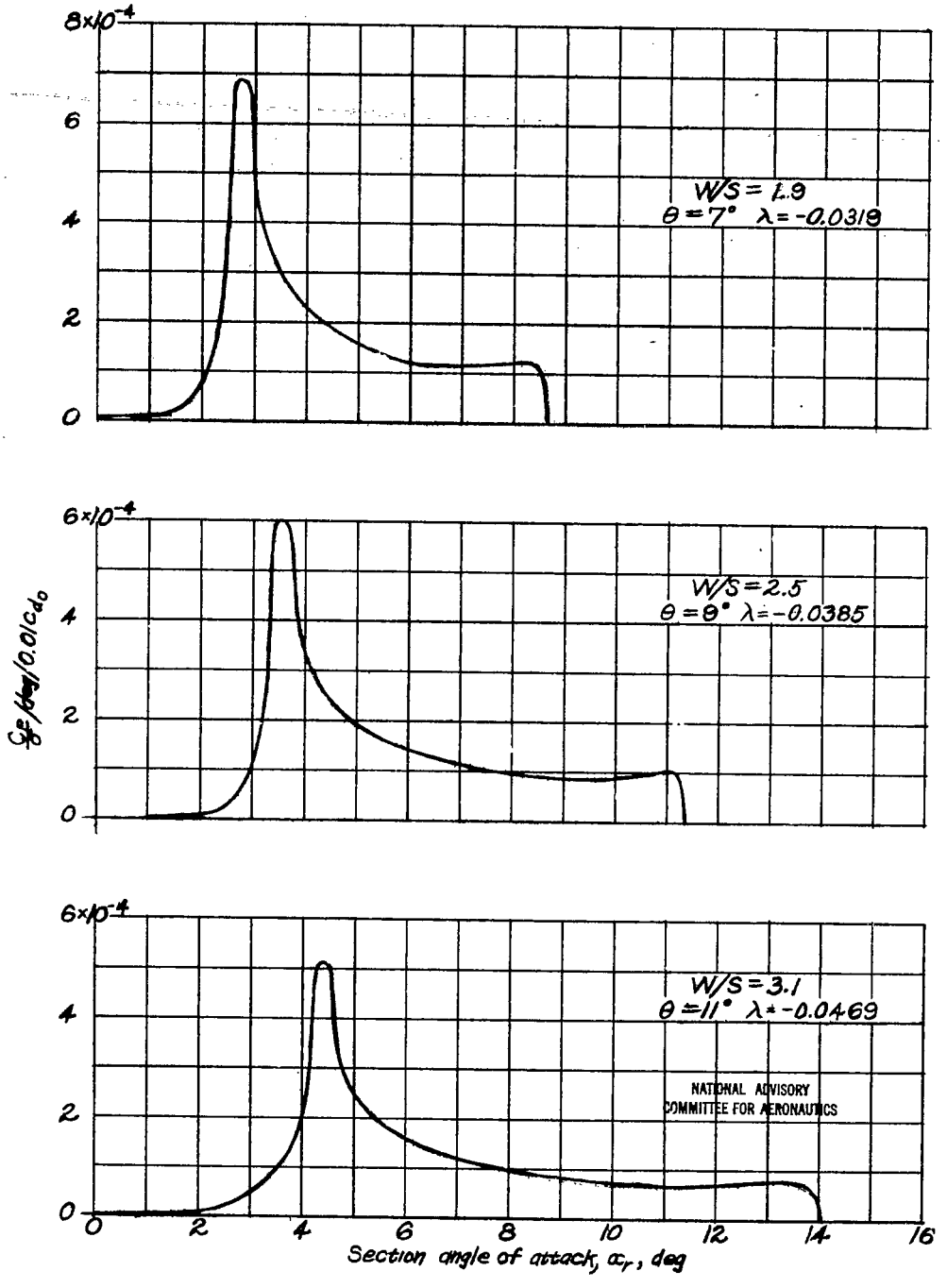

(b) Effect of loading. μ=0.2; σ=0.07; θ_1=0°.

Figure 9.- Continued. [redacted]

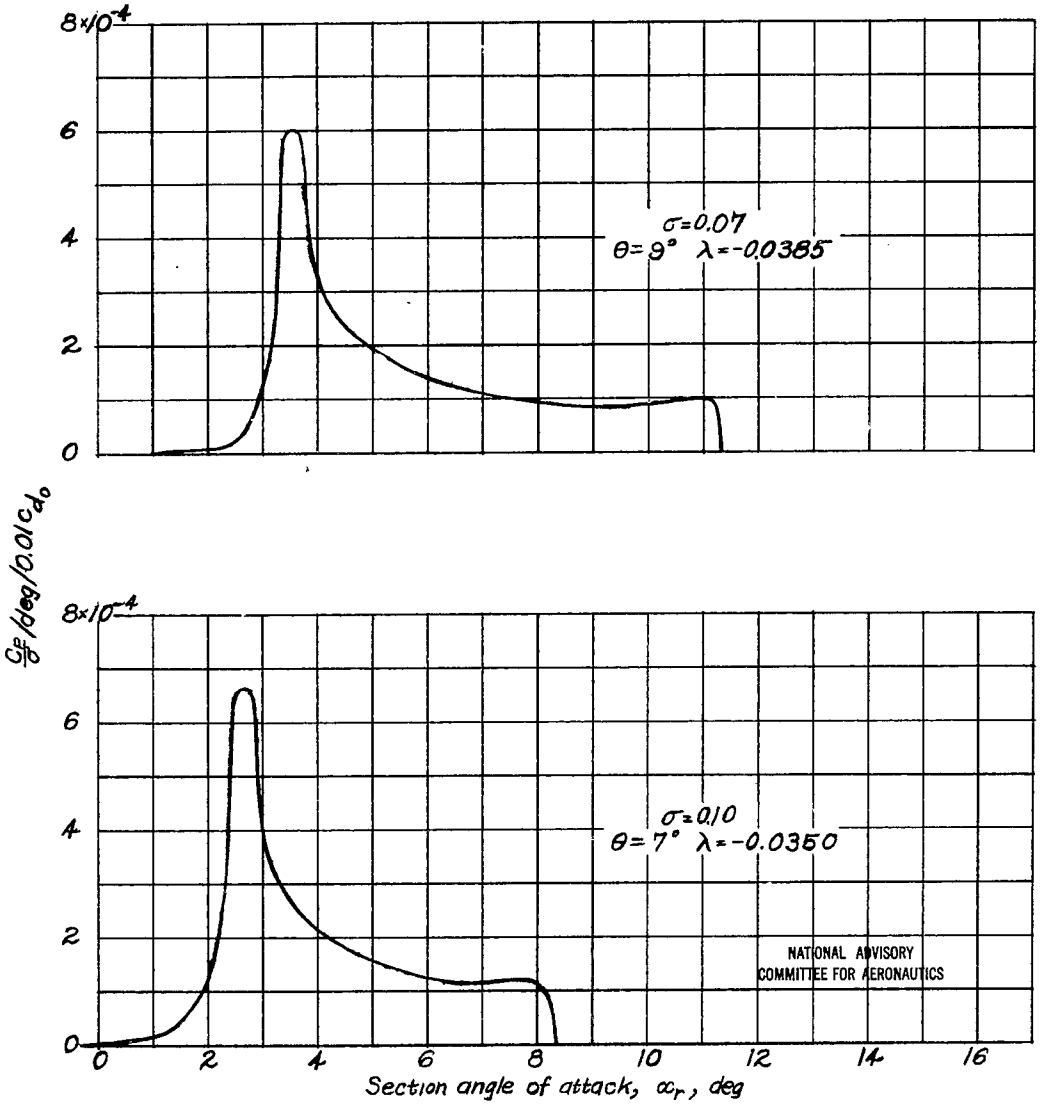

(c) Effect of solidity. μ=0.2; W/S=2.5; θ_1=0°.

Figure 9.- Continued.

[redacted]

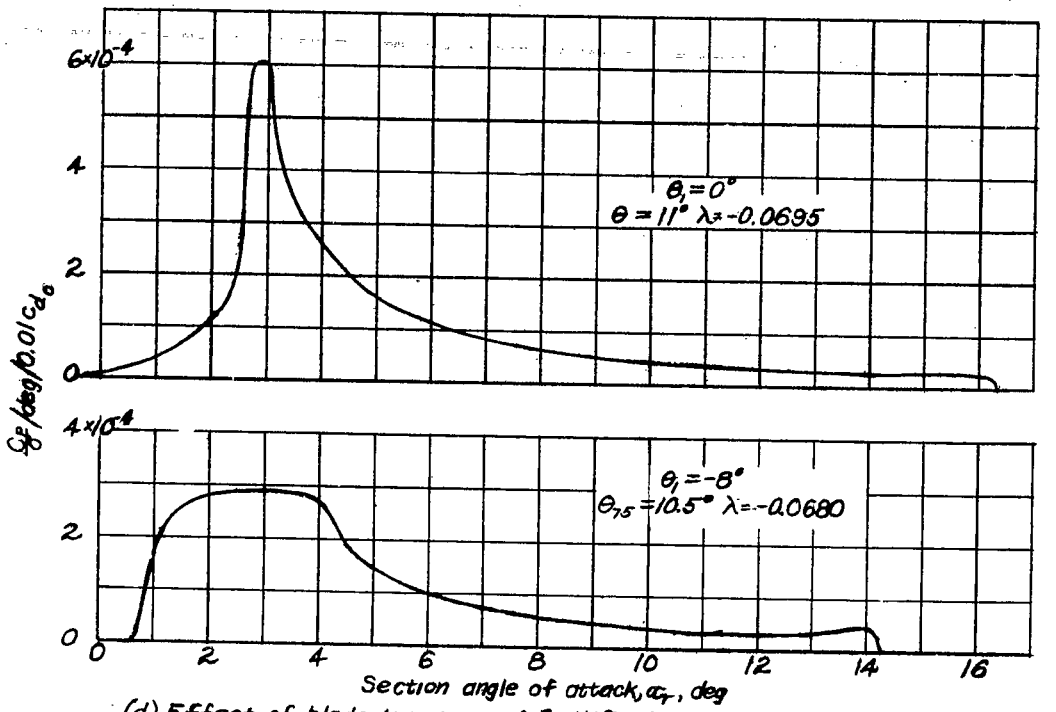

(d) Effect of blade twist. $\mu = 0.3$; $W/S = 2.5$; $\sigma = 0.07$.

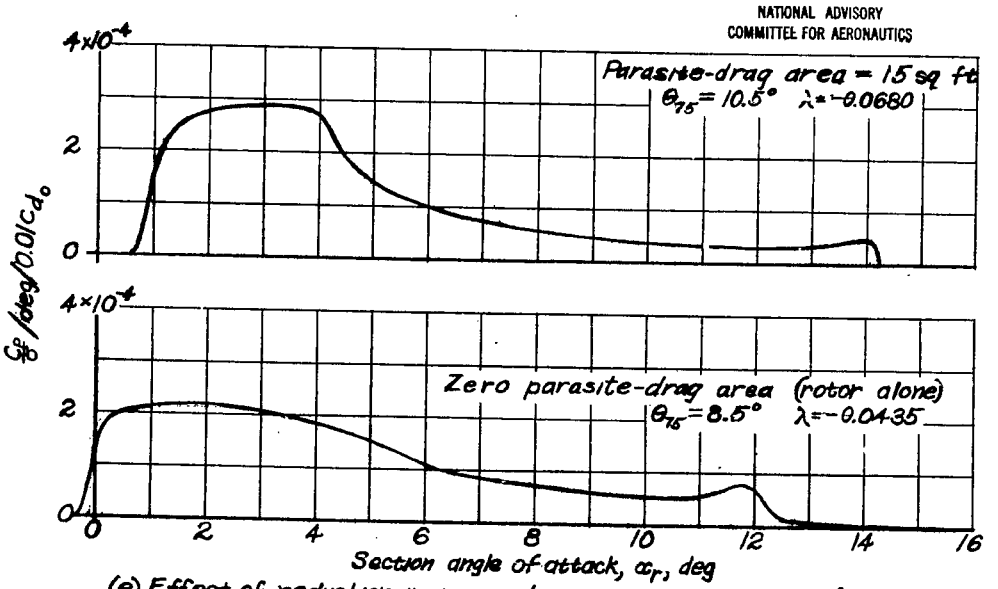

(e) Effect of reduction in required power input. $\mu = 0.3$; $W/S = 2.5$; $\theta_1 = -8°$.

Figure 9.- Concluded.

[redacted]

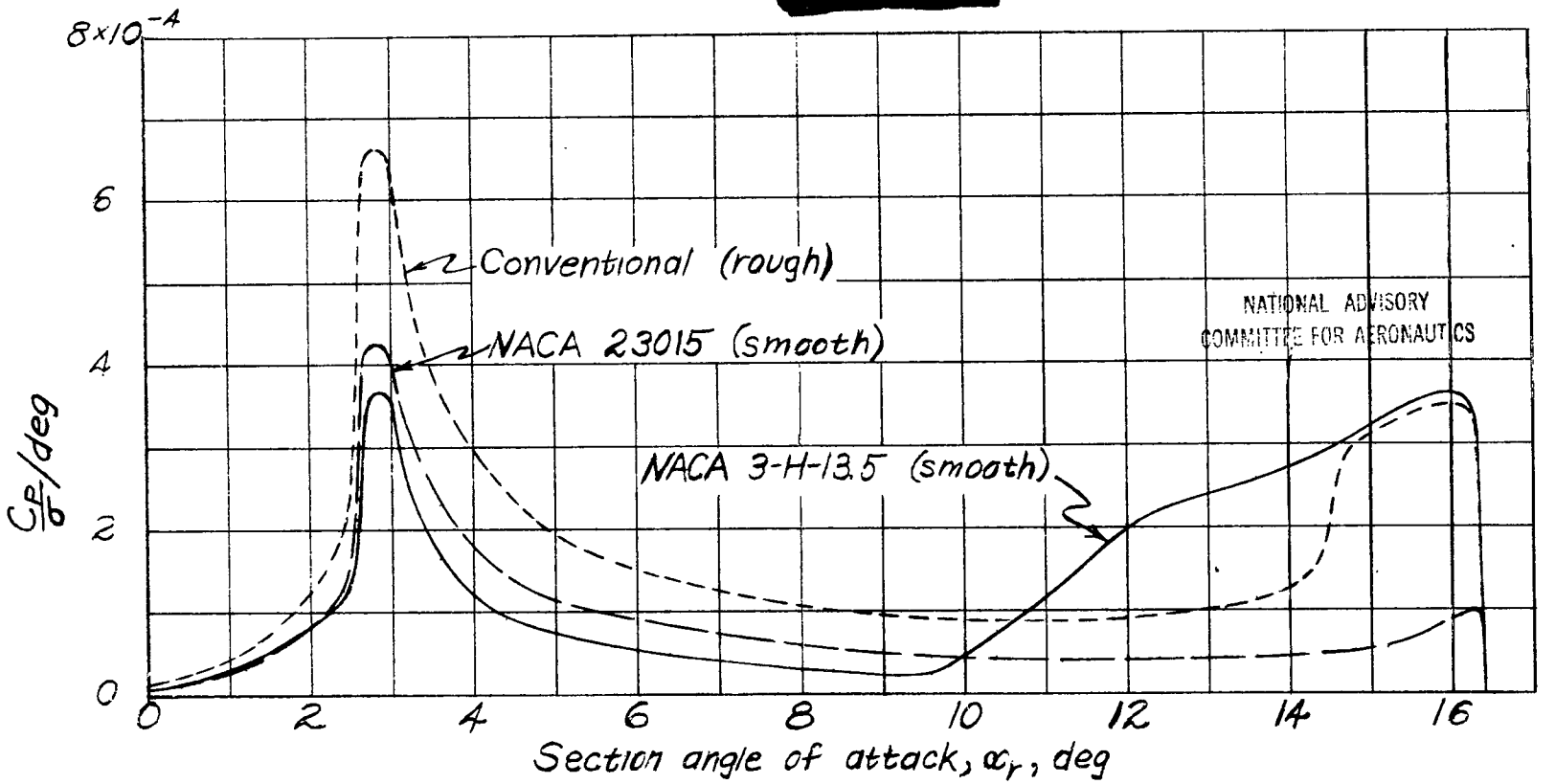

Figure 10.- Distribution of profile-drag power loss over the range of section angle of attack for each of the three airfoils when used in the sample helicopter rotor. $\mu=0.3$; $\theta=11°$; $\lambda=-0.0695$.

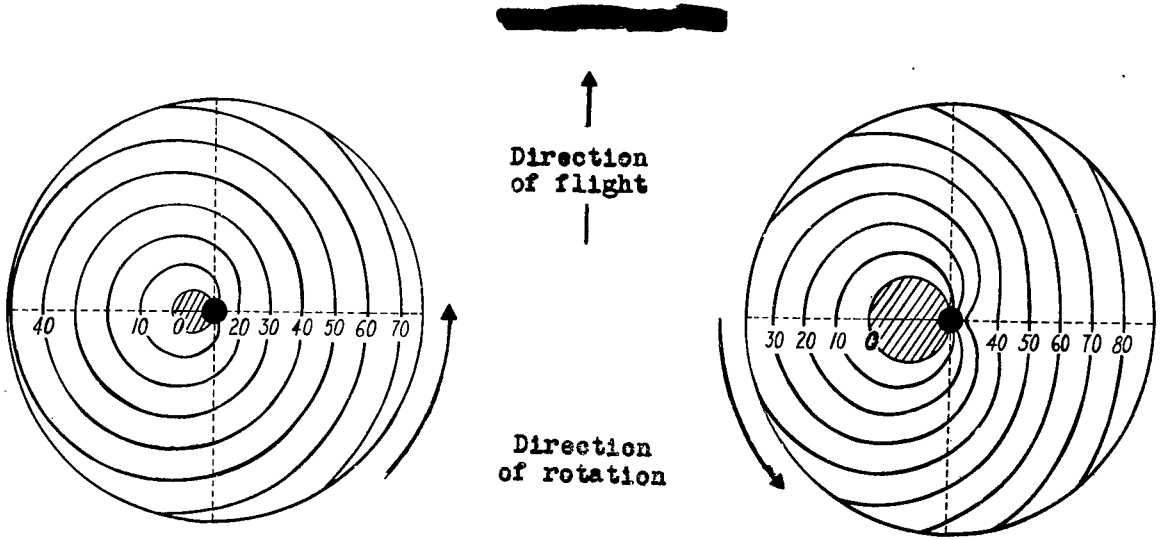

Figure 11.- Contours of Reynolds number for $\mu = 0.2$ and $\mu = 0.4$. Reynolds number equals $100\Omega Rc$ times value shown on contour. Values for standard conditions at sea level. For sample rotor, Reynolds number equals approximately 60,000 times values shown.

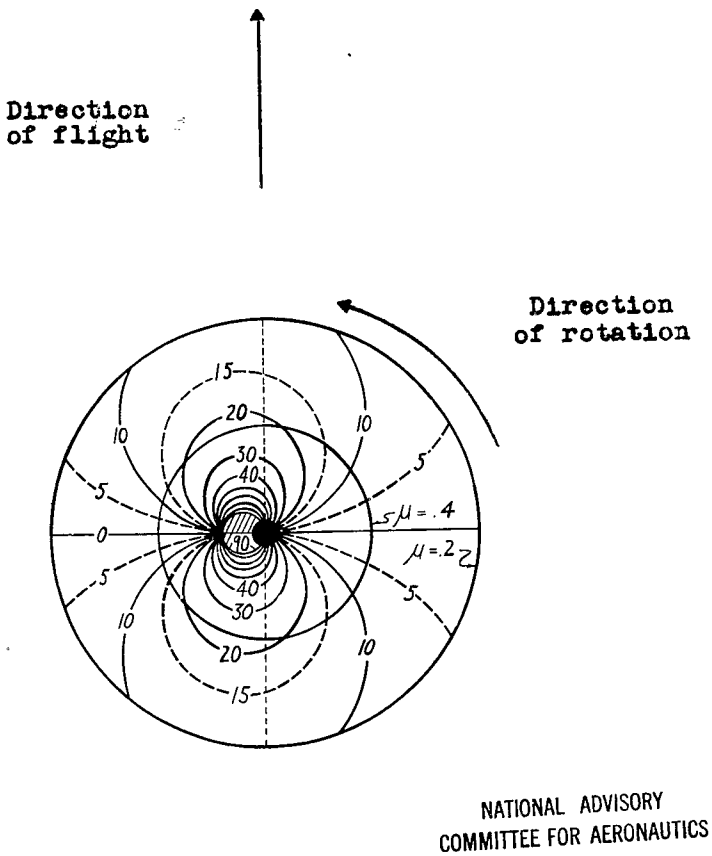

Figure 12.- Contours of rotor-blade angle of yaw for $\mu = 0.2$. Angles shown are in degrees. Contours may be used for any tip-speed ratio μ above 0.2 by placing a new rotor boundary ($x = 1.0$) at a radius equal to $0.2/\mu$ times the radius of the boundary shown for $\mu = 0.2$. As an example, the boundary for $\mu = 0.4$ has been drawn in.

TABLE I.- EFFECT OF VARIATIONS - Concluded

Figure	Conditions (a)			Profile-drag loss (hp)			
				For $c_{d_o} = 0.01$	For rough conventional section	For smooth NACA 23015 section	For smooth NACA 3-H-13.5 section
Effect of solidity							
	μ	σ					
9(c)	0.2	0.07		33.7	49.0	27.8	23.2
		.10		46.1	59.6	36.2	26.1
Effect of blade twist							
	μ	θ_1 (deg)					
9(d)	0.3	0		38.3	67.5	33.5	54.5
		-8		38.3	54.9	31.1	42.4
Effect of power input							
	μ	θ_1 (deg)	f (sq ft)				
9(e)	0.3	-8	15	38.3	54.9	31.1	42.4
			0	38.3	53.8	30.8	35.9

[a]All conditions not specified correspond to original assumptions.

NATIONAL ADVISORY
COMMITTEE FOR AERONAUTICS